THE JOURNAL OF BIOLOGICAL CHEMISTRY VOL. 289, NO. 45, pp. 31448–31457, November 7, 2014

The Crystal Structure of the Adenylation Enzyme VinN Reveals a Unique β-Amino Acid Recognition Mechanism*

Received for publication, August 1, 2014, and in revised form, September 17, 2014 Published, JBC Papers in Press, September 22, 2014, DOI 10.1074/jbc.M114.602326

Akimasa Miyanaga[‡], Jolanta Cieślak[§], Yuji Shinohara[§], Fumitaka Kudo[‡], and Tadashi Eguchi[§1]

From the Departments of [‡]Chemistry and [§]Chemistry and Materials Science, Tokyo Institute of Technology, O-okayama, Meguro-ku, Tokyo 152-8551, Japan

Background: The β-amino acid adenylation reaction is important for biosynthesis of natural products.
Results: We present the crystal structure and a mutational study of the adenylation enzyme VinN involved in vicenistatin biosynthesis.
Conclusion: VinN has a characteristic substrate-binding pocket that selectively accommodates β-amino acids.
Significance: This study could provide clues for β-amino acid specificity prediction and protein engineering of adenylation enzymes.

Adenylation enzymes play important roles in the biosynthesis and degradation of primary and secondary metabolites. Mechanistic insights into the recognition of α-amino acid substrates have been obtained for α-amino acid adenylation enzymes. The Asp residue is invariant and is essential for the stabilization of the α-amino group of the substrate. In contrast, the β-amino acid recognition mechanism of adenylation enzymes is still unclear despite the importance of β-amino acid activation for the biosynthesis of various natural products. Herein, we report the crystal structure of the stand-alone adenylation enzyme VinN, which specifically activates (2*S*,3*S*)-3-methylaspartate (3-MeAsp) in vicenistatin biosynthesis. VinN has an overall structure similar to that of other adenylation enzymes. The structure of the complex with 3-MeAsp revealed that a conserved Asp[230] residue is used in the recognition of the β-amino group of 3-MeAsp similar to α-amino acid adenylation enzymes. A mutational analysis and structural comparison with α-amino acid adenylation enzymes showed that the substrate-binding pocket of VinN has a unique architecture to accommodate 3-MeAsp as a β-amino acid substrate. Thus, the VinN structure allows the first visualization of the interaction of an adenylation enzyme with a β-amino acid and provides new mechanistic insights into the selective recognition of β-amino acids in this family of enzymes.

Adenylation enzymes, which include the nonribosomal peptide synthetase (NRPS)[2] adenylation domains, the acyl-CoA synthetases, and the luciferase enzymes, play important roles in the biosynthesis and degradation of primary and secondary metabolites (1). These enzymes first catalyze the adenylation of a carboxylate substrate using ATP to form an acyl-AMP intermediate. In most cases, the adenylation enzymes subsequently catalyze the formation of a thioester bond with the 4′-phosphopantetheine group of a carrier protein or CoA molecule. The carboxylate substrates of adenylation enzymes are structurally diverse and include acetate, amino acids, fatty acids, and aromatic acids. In general, each adenylation enzyme recognizes a specific carboxylate substrate.

Modular NRPS enzymes are involved in the biosynthesis of various secondary metabolites. NRPS adenylation domains, which mostly have α-amino acids as substrates, serve as gatekeepers of the NRPS assembly line via selective substrate recognition and activation. After the determination of the first crystal structure of an NRPS adenylation domain, PheA (see Fig. 1*A*) involved in gramicidin S biosynthesis (2), general rules for the assignment of substrate specificity for adenylation enzymes have been developed. These rules are based on classification of a specificity-conferring code derived from 10 amino acid residues that comprise the substrate-binding pocket (3, 4). The ~100-amino acid stretch of the N-terminal domain (corresponding to the positions Asp[235]–Cys[331] in PheA) contains nine of the 10 residues in the substrate-binding pocket. For α-amino acid substrate recognition, the Asp residue at the 235 position is invariant and is essential for stabilization of the α-amino group of the α-amino acid. The remaining residue is the highly conserved C-terminal Lys residue, which is involved in two key interactions with both the carboxylate group of the α-amino acid and the ribose moiety of adenylate. These two residues (Asp and Lys) are important to fix the position and orientation of the α-amino acid for the reaction. The other eight specificity-conferring code residues are involved in the recognition of the side chain of the α-amino acid substrate. This specificity-conferring code rule can be applied to various NRPS-type adenylation enzymes because information on the relationship between the sequence and substrate specificity of these enzymes has been accumulated (3–7). This rule allows us to predict the substrate specificity of many biochemically

* This work was supported in part by grants-in-aid for scientific research in innovative areas from the Japanese Ministry of Education, Culture, Sports, Science and Technology, grants-in-aid for young scientists (B) from the Japan Society for the Promotion of Science, the Nagase Science and Technology Foundation, and the Takeda Science Foundation.

The atomic coordinates and structure factors (codes 3WV4, 3WV5, and 3WVN) have been deposited in the Protein Data Bank (http://wwpdb.org/).

[1] To whom correspondence should be addressed: Dept. of Chemistry and Materials Science, Tokyo Inst. of Technology, 2-12-1 O-okayama, Meguro-ku, Tokyo 152-8551, Japan. Tel./Fax: 81-3-5734-2631; E-mail: eguchi@cms.titech.ac.jp.

[2] The abbreviations used are: NRPS, nonribosomal peptide synthetase; 3-MeAsp, 3-methylaspartate; r.m.s.d., root mean square deviation; VinNN, VinN N-terminal domain.

uncharacterized adenylation enzymes from their amino acid sequences and enables rational alteration of their substrate specificities (3, 8–12). However, this specificity-conferring code is not applicable for adenylation enzymes that activate unusual substrates such as β-amino acids.

Various natural products containing a β-amino acid unit have been isolated (13). In many cases, adenylation enzymes that activate β-amino acids are involved in their biosynthetic pathways (13–24). Similar to α-amino acid-activating enzymes, the interaction with the β-amino group and the carboxylate group should be important for β-amino acid-activating enzymes to fix the substrate orientation. However, the recognition model for α-amino acid-activating enzymes cannot be applied to that for β-amino acid-activating enzymes because the amino group position of the β-amino acid is different from that of the α-amino acid. Therefore, it can be assumed that β-amino acid adenylation enzymes have a structurally different active site for recognition of the β-amino acid. To date, no crystal structures of β-amino acid-activating enzymes are available, so the β-amino acid recognition mechanism of adenylation enzymes is poorly understood. What determines the substrate specificity between α-amino acid and β-amino acid adenylation enzymes also remains elusive.

Macrolactam natural products are an important class of macrocyclic polyketides, and many of them contain various β-amino acids at the starter position for polyketide chain elongation. Vicenistatin is produced by *Streptomyces halstedii* HC34 and belongs to the family of macrolactam antibiotics. This enzyme possesses a unique β-amino acid unit, 3-amino-2-methylpropionate, at the starter position of the polyketide backbone (25). Recently, we elucidated that the stand-alone adenylation enzyme VinN is involved in vicenistatin biosynthesis (14) (see Fig. 1*B*). VinN recognizes (2*S*,3*S*)-3-methylaspartate (3-MeAsp) as a β-amino acid substrate and catalyzes adenylation of the carboxyl group at the C4 position (see Fig. 1*A*). Then VinN transfers the β-amino acid group onto the stand-alone acyl carrier protein VinL to give 3-MeAsp-VinL. After decarboxylation of the 3-MeAsp moiety by the pyridoxal 5′-phosphate-dependent enzyme VinO, the resulting 3-amino-2-methylpropionate unit is aminoacylated with L-alanine to give dipeptidyl-VinL by another stand-alone adenylation enzyme, VinM. The dipeptide moiety is then selectively transferred onto the loading acyl carrier protein domain of polyketide synthase for polyketide chain elongation. Thus, VinN appears to play a crucial role in the selection of the β-amino acid starter unit for polyketide synthase in vicenistatin biosynthesis. Previous biochemical studies have shown that VinN exhibits a strong preference for 3-MeAsp over other amino acids (14). VinN shows no activity against α-amino acids except for weak activity against L-aspartate. As VinN exhibits relatively low sequence identity with well studied adenylation enzymes such as the NRPS adenylation domain, the substrate specificity of VinN cannot be predicted from the specificity-conferring code. The crystal structure of SlgN1, which catalyzes the adenylation of 3-MeAsp in the biosynthesis of streptolydigin, has been reported recently (26). SlgN1 recognizes (2*S*,3*S*)-3-MeAsp as an α-amino acid substrate and adenylates the carboxyl group at the C1 position (Fig. 1*A*). The orientation of 3-MeAsp at the active site in S1gN1 is proposed to be opposite to that in VinN. In this study, we carried out kinetic, mutational, and structural studies on VinN to clarify how VinN selectively recognizes 3-MeAsp. The VinN crystal structure allows the first visualization of the interaction between an adenylation enzyme and a β-amino acid and provides new mechanistic insights into the selective recognition of β-amino acids in this family of enzymes.

EXPERIMENTAL PROCEDURES

Preparation of Recombinant Wild-type and Mutant Enzymes—The N-terminal domain region of the *vinN* gene (*vinNN*) was amplified from pCold I-*vinN* (14) with the primers 5′-acgccatatcgccgaaagg-3′ and 5′-tttaagcttaccggccgccgaagtag-3′ and then inserted between the NdeI and HindIII sites of the expression vector pCold I (Takara Biochemicals, Ohtsu, Japan), which is designed to attach a hexahistidine-tagged sequence to the N terminus of the target protein.

Escherichia coli BL21(DE3) cells (Takara Biochemicals) harboring a pCold I-*vinN* or pCold I-*vinNN* plasmid were grown at 37 °C in Luria-Bertani broth containing ampicillin (50 μg/ml). After the optical density at 600 nm reached 0.6, protein expression was induced by the addition of isopropyl β-D-1-thiogalactopyranoside (0.2 mM), and the cells were then cultured for an additional 16 h at 15 °C. The recombinant protein, which was collected from cell-free extracts prepared by sonication, was purified on a TALON affinity column (Clontech). The protein was then desalted and concentrated using a PD-10 column (GE Healthcare) and an Amicon Ultra centrifugal filter (Merck Millipore, Billerica, MA), respectively. For crystallization, the recombinant protein was further purified by ResourceQ (GE Healthcare) anion-exchange chromatography with a linear gradient from 0.15 to 0.45 M NaCl in 10 mM HEPES-Na buffer (pH 7.7) containing 10% (v/v) glycerol.

For construction of the F231A, F231L, Y234A, S299A, M323G, K330A, K330N, and R331A mutants, the pCold I-*vinN* plasmid was used for site-directed mutagenesis. Site-directed mutagenesis was performed with a QuikChange site-directed mutagenesis kit (Stratagene, La Jolla, CA) using the following oligonucleotides: F231A, 5′-ggtctcctgggacgccggtctctacaagg-3′; F231L, 5′-ggtctcctggacctcggtctctacaagg-3′; Y234A, 5′-ggacttcggtctcgccaaggtgctgatctc-3′; S299A, 5′-cggatgttcaccaacgccgccgccgcg-3′; M323G, 5′-ccaggtcgtgcgcgggtacggccagaccg-3′; K330A, 5′-ccagaccgagtgcgcgcgcatctcgatc-3′; K330N, 5′-gccagaccgagtgcaatcgcatctcgatc-3′; R331A, 5′-gaccgagtgcaaggccatctcgatcatgcc-3′; and their complementary oligonucleotides. The mutations were confirmed by determining the nucleotide sequences. These plasmids were transformed into *E. coli* BL21(DE3) cells, and the mutated enzymes were prepared as described above. The CD experiment using a J-820 spectropolarimeter (Jasco, Tokyo, Japan) was performed to confirm that inactive mutant proteins such as M323G, K330A, and R331A adopt a fully folded state.

Enzyme Assays and Determination of Kinetic Parameters—A continuous spectroscopic assay that measures the release of inorganic pyrophosphate with the adenylation reaction was carried out according to the method of Webb (27). The assay solution (500-μl total volume) contained 50 mM Tris-HCl

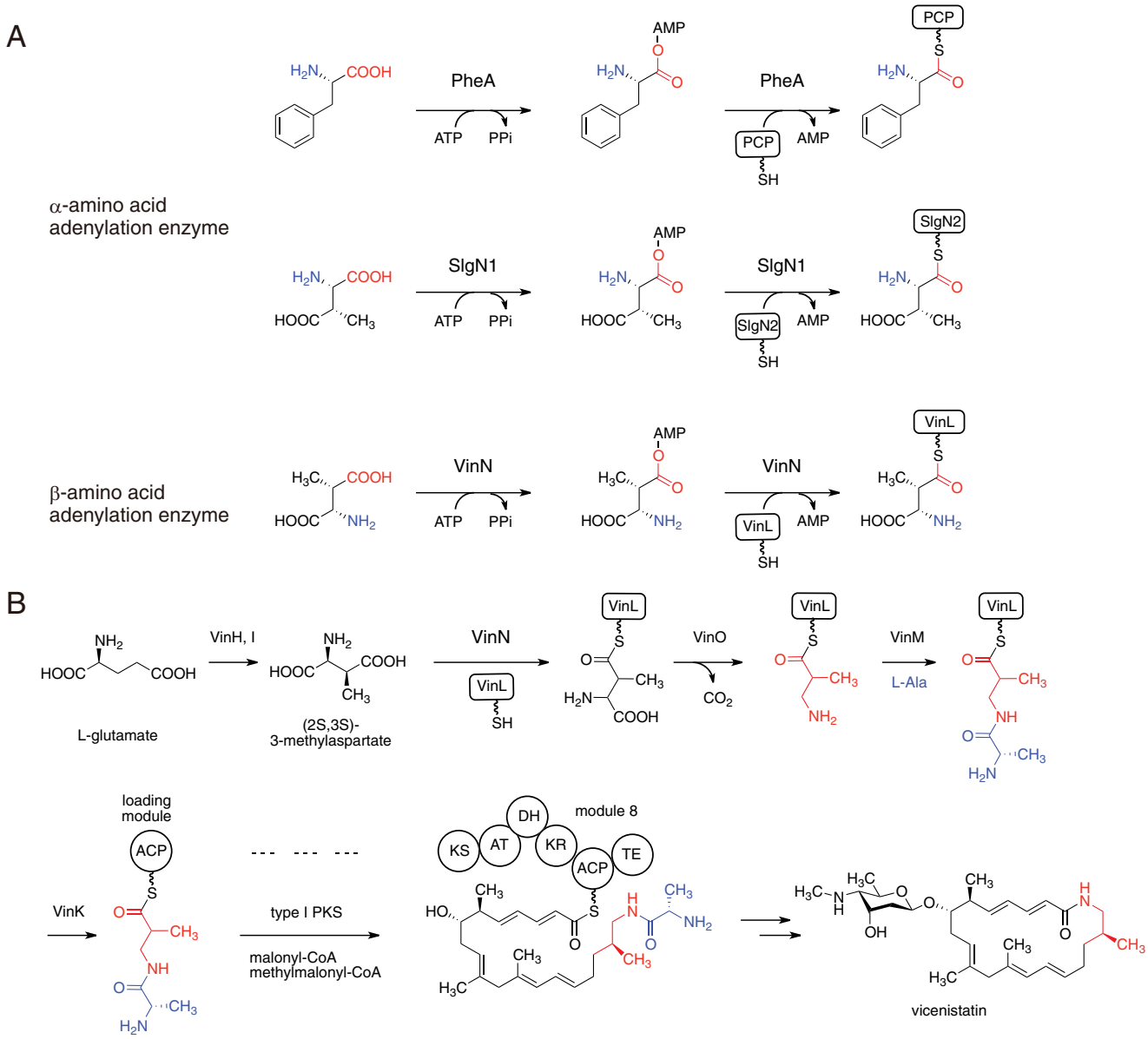

FIGURE 1. **Reaction of adenylation enzymes.** *A*, reactions of α-amino acid adenylation enzymes PheA and SlgN1 and β-amino acid adenylation enzyme VinN. *B*, biosynthetic pathway of vicenistatin, including the VinN reaction. The 3-amino-2-methylpropionate unit is shown in *red*. *ACP*, acyl carrier protein; *PKS*, polyketide synthase; *KS*, ketosynthase; *AT*, acyltransferase; *DH*, dehydratase; *KR*, ketoreductase; *TE*, thioesterase.

buffer (pH 7.5), 10% glycerol, 1 mM $MgCl_2$, 1 mM ATP, 0.1 mM 2-amino-6-mercapto-7-methylpurine ribonucleoside, 1 unit/ml inorganic pyrophosphatase, 1 unit/ml purine nucleotide phosphorylase, and 1 mM amino acid (DL-threo-β-MeAsp (Sigma-Aldrich) or L-aspartate (Kanto Chemical, Tokyo, Japan)). For kinetic assays, the amino acid concentration was varied between 0.04 and 100 mM. The reaction was initiated by addition of VinN (1–10 μM) to the mixture and incubated at 28 °C. The increase in absorbance at 360 nm, attributable to the formation of 2-amino-6-mercapto-7-methylpurine, per second was monitored using a UV-2450 spectrophotometer (Shimadzu, Tokyo, Japan). The initial velocity was determined from the linear portion of the optical density profile ($\epsilon_{360\,nm} = 11{,}000\ M^{-1}\ cm^{-1}$). Steady-state parameters were determined by the Michaelis-Menten equation.

Crystallization, Data Collection, and Structure Determination—Crystals of VinNN were grown from a 1:1 (v/v) mixture of a VinNN protein solution (10 mg/ml in 10 mM HEPES-Na (pH 7.5) and 10% glycerol) and a reservoir solution (0.1 M Tris-HCl (pH 8.5), 0.2 M sodium acetate, and 30% polyethylene glycol 4000) using the sitting drop vapor diffusion method at 5 °C. The 3-MeAsp complex and L-aspartate complex were prepared by soaking apocrystals in 100 mM DL-threo-β-MeAsp for 4 h and 100 mM L-aspartate for 1 h, respectively. Prior to collection of the x-ray data, the crystals were flash frozen in a stream of liquid nitrogen. The x-ray diffraction data were collected on beamlines BL-5A and AR-NW-12A at the Photon Factory (Tsukuba, Japan) and subsequently indexed, integrated, and scaled using the iMosflm program (28). The initial phases were determined by the molecular replacement method using the Molrep pro-

TABLE 1
Kinetic analysis of VinN wild type and mutants

Enzymes	Substrate	K_m	k_{cat}	k_{cat}/K_m
		mM	min^{-1}	$min^{-1}\ M^{-1}$
Wild type	3-MeAsp	0.13 ± 0.02	0.39 ± 0.01	3000
F231L	3-MeAsp	0.96 ± 0.24	0.095 ± 0.006	99
S299A	3-MeAsp	0.77 ± 0.08	0.14 ± 0.03	180
Wild type	L-Aspartate	4.5 ± 0.5	0.79 ± 0.02	180
F231L	L-Aspartate	19 ± 5	0.27 ± 0.02	14
S299A	L-Aspartate	18 ± 5	0.12 ± 0.01	6.7

gram (29) with the crystal structure of the N-terminal domain of 4-coumarate-CoA ligase from *Populus tomentosa* (Protein Data Bank code 3A9U) used as a search model. Rotation and translation functions were calculated using data of 50.0–2.5-Å resolution. Two molecules were found in the asymmetric unit (the correlation coefficient of the correct solution is 0.365, which is significantly higher than those of other unrelated peaks). The ARP/wARP program (30) was used for automatic initial protein model building. Coot (31) was used for visual inspection and manual rebuilding of the model. Refmac (32) was used for refinement. The figures were prepared using PyMOL (33). The distances were measured in both molecules in the asymmetric unit and then shown as averaged values. The geometries of the final VinNN structures were evaluated using the program Rampage (34). The resulting coordinates and structure factors have been deposited in the Protein Data Bank (Protein Data Bank codes 3WV4, 3WV5, and 3WVN).

RESULTS

Kinetic Analysis of VinN—To analyze the preference of VinN for 3-MeAsp, we carried out a kinetic analysis. The K_m value for DL-*threo*-3-MeAsp, which is a mixture of 2*S*,3*S*- and 2*R*,3*R*-enantiomers, at 28 °C was found to be 0.13 ± 0.02 mM, which is comparable with those of the known adenylation enzymes (15–17, 35, 36) (Table 1). VinN also shows weak activity toward L-aspartate, which lacks the methyl group at the C3 position. VinN had a 35-fold larger K_m value for L-aspartate (4.5 ± 0.5 mM). Thus, the methyl group at the C3 position of 3-MeAsp is important for recognition by VinN. VinN showed no activity against D-aspartate, indicating that the orientation of the functional groups at the β-position of 3-MeAsp is important for recognition by VinN. These results suggest that VinN accepts only (2*S*,3*S*)-3-MeAsp as a substrate in the reaction with DL-*threo*-3-MeAsp.

Crystallization of VinN—To investigate the structural basis of the β-amino acid recognition mechanism, we carried out a crystallographic analysis of VinN. We first attempted to crystallize the full-length VinN protein. However, we could not obtain any VinN crystals. Adenylation enzymes have been reported to change conformation at the C-terminal region during reaction (37). After the initial adenylation step, the C-terminal domain region is rotated by ~140° for the following thioester bond formation step. Crystallization of these enzymes containing flexible C-terminal parts is challenging. Hence, there are some examples of crystal structures in which only the N-terminal part has been used for crystallization (26, 38, 39). Therefore, we constructed the heterologous expression system of the VinNN protein containing only the N-terminal domain (Met^1–Arg^{426}) and then attempted to crystallize the VinNN protein. Finally, we succeeded in the crystallization of VinNN and determined its crystal structure at 2.15-Å resolution (Table 2).

Overall Structure of VinN—Two VinNN molecules are present in each crystallographic asymmetric unit. The VinNN structure has a five-layered αβαβα sandwich fold as observed in other crystal structures of adenylation enzymes (2, 26, 38–41) (Fig. 2*A*). The structure contains a few disordered surface loop regions (Met^1–Lys^{23}, Gly^{250}–Asp^{254}, and Asp^{399}–Gly^{403}). A search for structurally related proteins using the Dali program (42) revealed that the closest functionally characterized protein is fatty acyl-CoA synthetase FadD13 (40) (Protein Data Bank code 3T5C, *Z* score = 49.8, root mean square deviation (r.m.s.d.) of 1.7 Å for 372 Cα atoms, and sequence identity of 23%). VinNN is also structurally similar to NRPS adenylation domains, including PheA (2) (Protein Data Bank code 1AMU, *Z* score = 45.7, r.m.s.d. of 2.0 Å for 365 Cα atoms, and sequence identity of 20%) and SlgN1 (26) (Protein Data Bank code 4GR5, *Z* score = 42.9, r.m.s.d. of 2.1 Å for 362 Cα atoms, and sequence identity of 23%).

A structural comparison of VinNN with other adenylate-bound adenylation enzymes, including PheA and SlgN1 (2, 26, 35, 41, 43), showed that VinNN has a similar cleft for adenylate binding on the surface of the N-terminal domain. VinN has several conserved residues at that cleft (Fig. 3). For example, Thr^{327} and Glu^{328} that are supposed to interact with the α-phosphate moiety of adenylate, Asp^{411} that is supposed to interact with ribose hydroxyl groups, and Tyr^{324} that is supposed to interact with the adenine moiety are located at almost the same positions in the structure (Fig. 4*A*). These structural observations suggest that the manner of ATP binding of VinN is similar to that of other adenylation enzymes.

Structure of the 3-MeAsp and L-Aspartate Complexes—To understand the substrate recognition mechanism of VinN, we determined the structure of the complex with 3-MeAsp at 2.20-Å resolution. The position of the substrate-binding pocket of VinNN is similar to those of other adenylation enzymes. The entrance of the substrate-binding pocket is exposed to solvent because of the absence of the C-terminal domain. The structure shows clear electron density for (2*S*,3*S*)-3-MeAsp in the substrate-binding pocket but not for (2*R*,3*R*)-3-MeAsp (Fig. 2*B*). The binding of 3-MeAsp occurred with little overall structural perturbation to the VinNN polypeptide backbone (r.m.s.d. of 0.47 Å for 385 Cα atoms of chain A). Some side-chain movements are observed in the binding pocket. The side chains of Asp^{230}, Phe^{231}, and Ser^{299} exhibit 19°, 15°, and 140° rotations, respectively, to accommodate 3-MeAsp (Fig. 2*C*). In the substrate-free structure, the backbone and side chains in the region of Ser^{299} and Ala^{300} seem to be flexible judging from their high B-factor values (65.5 $Å^2$). In contrast, this region of the structure in the complex exhibits significantly lower B-factor values (33.0 $Å^2$), suggesting that the binding of 3-MeAsp stabilizes it. Furthermore, we determined the structure of the complex with L-aspartate at 2.20-Å resolution. Similarly, the electron density of L-aspartate was clearly observed in the substrate-binding pocket (Fig. 2*D*). The overall structure of the complex with L-aspartate is almost identical to that with 3-MeAsp (r.m.s.d. of

TABLE 2
Data collection and refinement statistics

	Data set		
Protein Data Bank code	**Apo 3WV4**	**3-MeAsp complex 3WV5**	**L-Aspartate complex 3WVN**
Data collection statistics			
Beamline	PF BL-5A	PF AR-NW12A	PF AR-NW12A
Wavelength (Å)	0.9782	1.0000	1.0000
Space group	$C222_1$	$C222_1$	$C222_1$
Unit cell parameters			
a (Å)	81.79	80.66	80.53
b (Å)	109.82	109.41	109.30
c (Å)	201.46	200.21	200.07
Resolution (outer shell) (Å)	50.00-2.15 (2.21-2.15)	37.41-2.20 (2.28-2.20)	42.27-2.20 (2.32-2.20)
Unique reflections	44,155 (3,311)	44,288 (4,087)	43,099 (5,734)
Redundancy	5.7 (4.7)	6.7 (6.1)	6.1 (5.5)
Completeness (%)	89.5 (83.5)	97.8 (93.6)	95.5 (88.3)
R_{merge} (%)	7.3 (57.3)	6.3 (47.2)	7.5 (61.0)
Mean $I/\sigma(I)$	12.2 (2.3)	17.0 (3.4)	15.5 (2.6)
Wilson B-factor (Å^2)	31.6	32.5	32.8
Refinement statistics			
Resolution (Å)	50.00-2.15	37.41-2.20	39.63-2.20
Reflections used ($F > 0\sigma F$)	44,123	44,244	43,055
R_{work} (%)	20.2	20.5	20.7
R_{free} (%)	24.5	24.5	24.3
No. of non-hydrogen atoms			
Protein	5,845	5,690	5,669
Water	191	203	176
Substrate	0	20	18
Average B-factors (Å^2)			
Protein	43.9	45.0	45.5
Water	39.8	45.6	44.5
Substrate		33.9	43.6
r.m.s.d. from ideality			
Bond lengths (Å)	0.016	0.016	0.015
Bond angles (°)	1.71	1.75	1.73
Ramachandran plot			
Favored region (%)	98.3	98.9	98.3
Allowed region (%)	1.7	1.0	1.7
Outer region (%)	0.0	0.1	0.0

0.13 Å for 388 Cα atoms of chain A). There are no significant displacements in the substrate-binding pocket between the structures of these two complexes (Fig. 2*C*).

Substrate Binding in the Complex Structures—In both complex structures, the amino acid substrate is bound to the substrate-binding pocket of VinNN in the same position and orientation. The C4 carboxyl group of 3-MeAsp and L-aspartate is exposed to solvent and does not interact with any residues of the N-terminal domain.

In the structure of the complex with 3-MeAsp, two salt bridge interactions are formed between Arg^{331} and the C1 carboxyl group of 3-MeAsp (2.7 and 2.8 Å), and one salt bridge interaction is observed between Lys^{330} and the C1 carboxyl group of 3-MeAsp (3.0 Å) (Fig. 2*B*). These structural observations suggest the importance of Lys^{330} and Arg^{331} in 3-MeAsp recognition. In fact, the K330N mutant showed a significantly decreased activity (0.8% of the wild type). In addition, K330A and R331A mutants showed a complete loss of activity. Both Lys^{330} and Arg^{331} side chains are stacked between Tyr^{234} and Met^{323} and are located close together (3.5 Å) despite an electrostatic repulsion (Fig. 2*E*). Even in the substrate-free structure, these basic residues occupy the same position (Fig. 2*C*). Tyr^{234} and Met^{323} do not directly interact with the 3-MeAsp substrate but are likely to modulate the conformation of the Lys^{330} and Arg^{331} side chains by steric effects. To evaluate this steric effect of Tyr^{234} and Met^{323}, we constructed Y234A and M323G mutants. The Y234A mutant showed very weak activity (3.7% of the wild type), and the M323G mutant completely lost activity. In these mutants, the smaller side chain of the mutated residue cannot have any steric interactions with the Lys^{330} or Arg^{331} side chains. This probably causes displacement of these basic residues to reduce the electrostatic repulsion between them, resulting in the observed significant reduction in activity.

Ser^{299} forms a hydrogen bond with the C1 carboxyl group of 3-MeAsp. The S299A mutant exhibited a 6-fold higher K_m value compared with the wild type, suggesting that the side-chain hydroxyl group of Ser^{299} participates in the recognition of the C1 carboxyl group of 3-MeAsp. The side-chain carboxyl group of Asp^{230} interacts with the β-amino group of the 3-MeAsp substrate with a salt bridge interaction (2.6 Å). The main-chain carbonyl oxygen of Lys^{330} also interacts with the β-amino group through a hydrogen bond (2.8 Å). The methyl group of 3-MeAsp seems to be recognized by the side-chain aromatic group of Phe^{231} (3.8–4.3 Å) through CH-π (44) and van der Waals interactions (Fig. 2, *C* and *E*). The presence of these interactions appears to give 3-MeAsp selectivity over L-aspartate. In the structure of the complex with L-aspartate, the C3 carbon of L-aspartate is relatively far from the side chain of Phe^{231} (5.0 Å). F231A and F231L mutations resulted in higher K_m values for both 3-MeAsp and L-aspartate. The F231L mutant showed a 7-fold higher K_m value for 3-MeAsp compared with the wild type, although the Leu residue should retain the van der Waals interactions with the methyl group of 3-MeAsp. This mutant also showed a 4-fold higher K_m value for

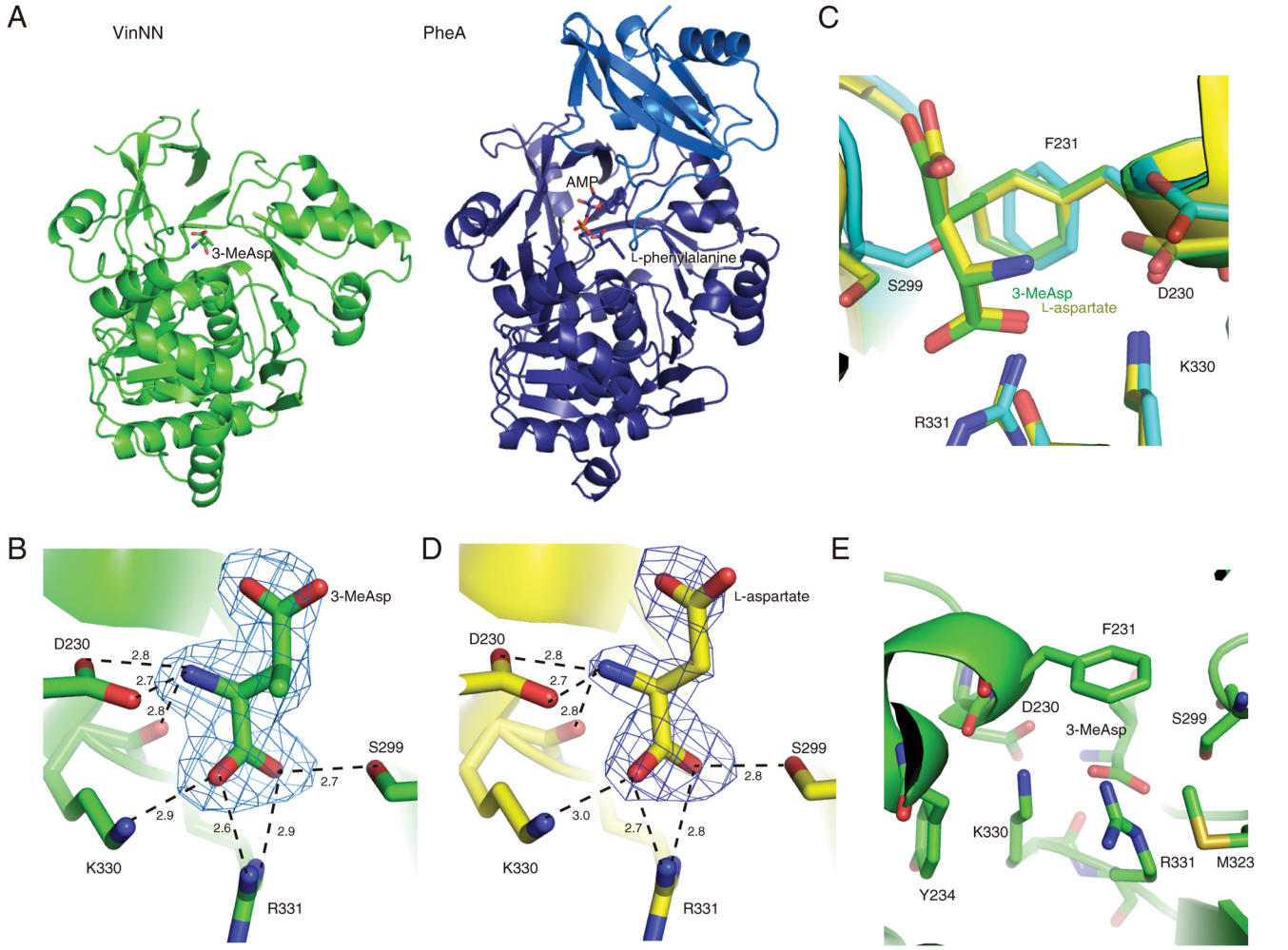

FIGURE 2. **Structure of VinNN.** *A*, overall structures of VinNN (*left*) and PheA (*right*). The ligand molecules are shown as *stick* models. The N-terminal domain and C-terminal domain of PheA are shown in *purple* and *blue*, respectively. *B*, the substrate-binding pocket of the complex with 3-MeAsp. An $F_o - F_c$ electron density map contoured at 3.0σ was constructed prior to incorporation of the 3-MeAsp molecule. Interactions with 3-MeAsp are shown as *broken lines*. *C*, superimposition of the 3-MeAsp complex structure (*green*), L-aspartate complex structure (*yellow*), and the substrate-free structure (*cyan*). *D*, the substrate-binding pocket of the complex with L-aspartate. An $F_o - F_c$ electron density map contoured at 3.0σ was constructed prior to incorporation of the L-aspartate molecule. Interactions with L-aspartate are shown as *broken lines*. *E*, the substrate-binding pocket of the complex with 3-MeAsp viewed from the base of the pocket. Seven residues that are directly or indirectly involved in the substrate binding are shown.

L-aspartate (Table 1). Furthermore, the F231A mutant exhibited very weak activity toward 3-MeAsp (1.8% of the wild type) and no detectable activity with L-aspartate. These results suggest that the mutation of Phe^{231} affects substrate specificity both for 3-MeAsp and L-aspartate. The side chain of Phe^{231} might be important for the recognition of not only the methyl group but also other parts of 3-MeAsp.

Structural Comparison with the Crystal Structures of Other Adenylation Enzymes—We compared the structure of VinNN with those of other adenylation enzymes, including PheA, which recognizes L-phenylalanine as a substrate (2). The carboxyl group at the C4 position of 3-MeAsp that is adenylated in VinN occupies a position similar to that of the α-carboxyl group of L-phenylalanine in PheA (Fig. 4*B*), suggesting that the same interaction exists with the conserved Lys residue of the C-terminal domain (Lys^{510} in VinN) as observed in other adenylation enzymes (Fig. 5). The position of the amino nitrogen atom of 3-MeAsp is similar to that of L-phenylalanine in PheA. In both structures, the conserved Asp residue forms the same interaction with the amino group of the substrate. Thus, the distance between the amino and carboxylate groups of the amino acids at the active site of both enzymes is similar, although the β-amino acid has one carbon atom inserted between these termini compared with the α-amino acid. Consequently, in the VinNN structure, the C2–C3 bond of 3-MeAsp appears to be pushed into a relatively large space of the active site. The positions of the three carbon atoms (C1, C2, and C3) of 3-MeAsp individually show 1.1–1.5-Å displacement from the corresponding atoms of L-phenylalanine in the PheA structure.

Further structural comparisons revealed that two factors likely give rise to the difference in the overall architecture of the substrate-binding pocket. First, the β13β14 loop containing the two important residues Lys^{330} and Arg^{331} is one residue shorter in VinN than in most other adenylation enzymes, including PheA (Figs. 3 and 4*C*). This one-residue-shorter loop has also been reported in malonyl-CoA synthetase ScMatB (45). In the VinNN structure, this shorter loop causes a 0.8–2.0-Å movement of the polypeptide backbone between Lys^{330} and Ile^{332} (Fig. 4, *B* and *D*), providing space for fixing the location and

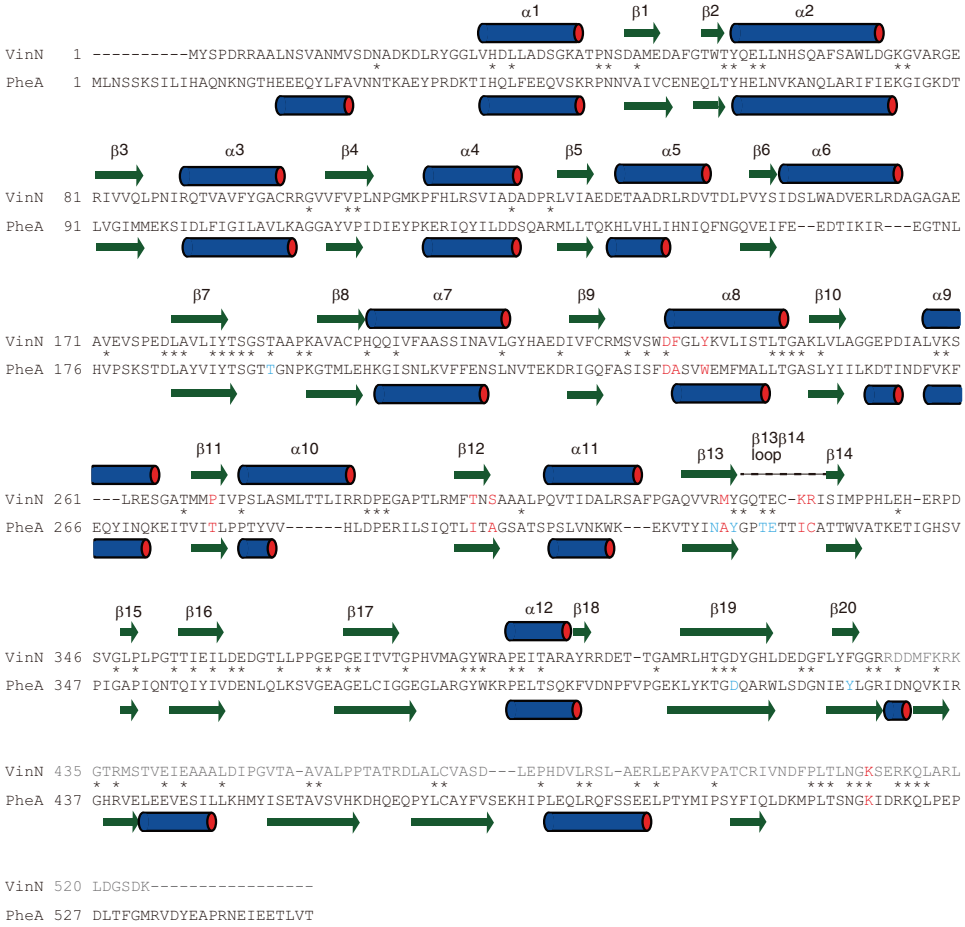

FIGURE 3. **Amino acid sequence comparison of VinN with PheA.** Specificity-conferring code residues are shown in *red*. The residues involved in AMP binding in PheA are shown in *blue*. The secondary structural elements of VinNN and PheA are indicated by *bars* above or below the sequence. The VinN $\beta13\beta14$ loop containing Lys^{330} and Arg^{331} is indicated by a *broken line* above the sequence. The C-terminal domain sequence of VinN is shown in *gray*. The conserved positions are marked with an *asterisk*.

orientation of the C1–C2 bond of 3-MeAsp. The C1 carboxyl group of 3-MeAsp might be pulled in this space by interactions with Ser^{299}, Lys^{330}, and Arg^{331}, resulting in its slight movement toward the $\beta13\beta14$ loop. Second, VinN has bulky residues in the substrate-binding pocket. Phe^{231} and Ser^{299}, which are equivalent to Ala^{236} and Ala^{301}, respectively, in PheA, are located on the opposite side of the substrate-binding pocket from the $\beta13\beta14$ loop (Fig. 4*B*). The position of the C1, C2, and C3 carbon atoms of the 3-MeAsp substrate could be affected by the presence of these two larger residues. They might be pushed toward the $\beta13\beta14$ loop by the steric constraints of these residues. The importance of Phe^{231} was confirmed by the mutational studies where mutation of Phe^{231} significantly reduced the activity against both 3-MeAsp and L-aspartate (Table 1). Thus, these two factors are thought to be important for the construction of a β-amino acid-specific substrate-binding pocket to accommodate 3-MeAsp.

DISCUSSION

Many crystal structures of adenylation enzymes such as NRPS adenylation domains have been reported (2, 26, 35, 41, 43, 46–48). However, no crystal structure of a β-amino acid-activating enzyme has been available so far. In this study, we determined the structure of the N-terminal domain of VinN, which is involved in biosynthesis of the macrolactam antibiotic vicenistatin. The structures of complexes with both 3-MeAsp and L-aspartate clearly demonstrate that VinN recognizes 3-MeAsp as a β-amino acid. The VinNN structure can provide important mechanistic insights into β-amino acid recognition as described below.

Sequence alignment and structural comparison with other adenylation enzymes revealed that the β-amino acid substrate specificity of VinN is also governed by the specificity-conferring code (Figs. 3 and 5). The VinNN structure and the mutational study clearly show that five of the 10 residues (Asp^{230}, Phe^{231}, Ser^{299}, Lys^{330}, and Arg^{331}) are directly involved in substrate binding (Fig. 2, *B* and *E*). Two other residues (Tyr^{234} and Met^{323}) derived from the specificity-conferring code seem to be indirectly involved in substrate binding by conformational modulation of two essential basic residues, Lys^{330} and Arg^{331}. In addition, the conserved Lys^{510} of the C-terminal domain is thought to interact with the substrate carboxyl group that is adenylated as reported for other adenylation enzymes. Importantly, the Asp residue important for recognition of the α-amino group of the α-amino acid is also conserved in VinN. The VinNN structure shows that Asp^{230} is used for the recognition of the β-amino group of 3-MeAsp. However, the overall archi-

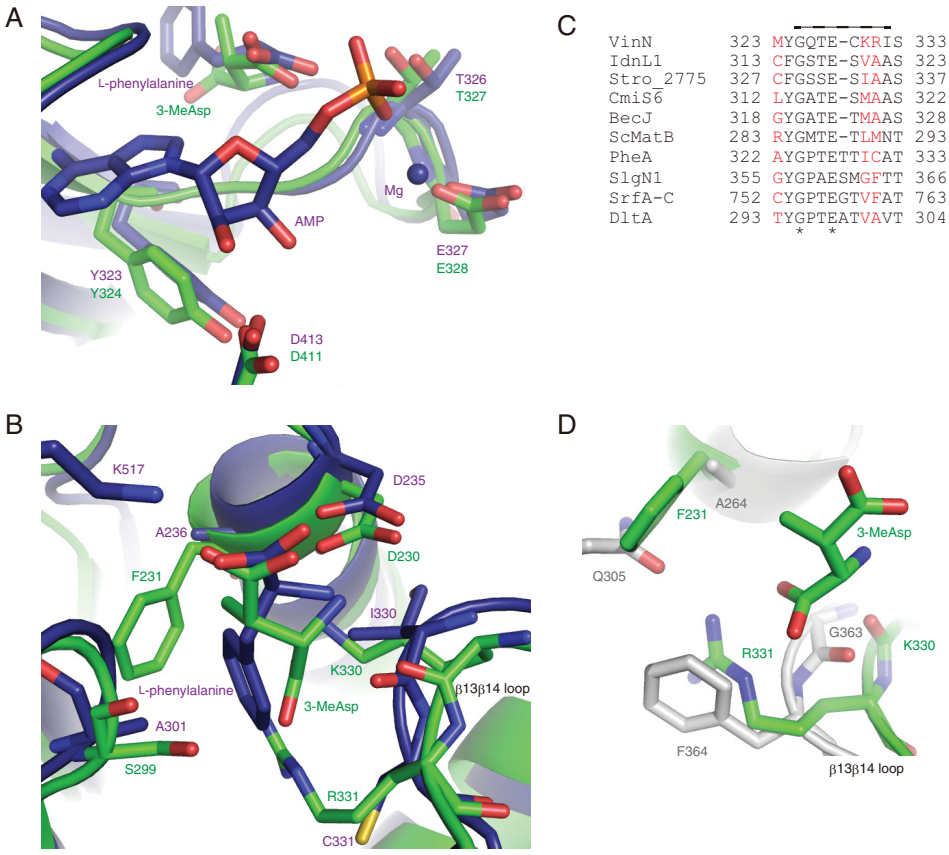

FIGURE 4. **Structural comparison of VinNN with other adenylation enzymes.** *A*, the structure of the adenylate-binding site. The superimposed structures of VinNN (*green*) and PheA (*purple*) are shown. *B*, the structure of the substrate-binding pocket. The superimposed structures of VinNN (*green*) and PheA (*purple*) are shown. *C*, the alignment of the β13β14 loop region of VinN with other adenylation enzymes. The sequences of the following 10 adenylation enzymes were used for the alignment analysis: α-amino acid-activating enzymes, including *Bacillus brevis* PheA (2), *Streptomyces lydicus* SlgN1 (26), *Bacillus subtilis* SrfA-C (45), and *Bacillus cereus* DltA (35); β-amino acid-activating enzymes, including VinN, *Streptomyces* sp. ML694-90F3 IdnL1 (18), *Salinispora tropica* Stro_2775 (21), *Streptomyces* sp. MJ635-86F5 CmiS6 (19), and *Streptomyces* sp. DSM 21069 BecJ (20); and malonyl-CoA synthetase *Streptomyces coelicolor* ScMatB (44). The specificity-conferring code residues are shown in *red*. The VinN β13β14 loop is indicated by a *broken line* above the sequence. The conserved positions are marked with an *asterisk*. *D*, the superimposed substrate-binding pocket structures of VinNN (*green*) and SlgN1 (*gray*).

tecture of the substrate-binding pocket of VinN is significantly different compared with those of other adenylation enzymes. The β-amino acid specificity of VinN seems to be dictated by the surrounding regions, including the shorter β13β14 loop and the specificity-conferring code residues such as Phe^{231}. These factors seem to largely contribute to control of the conformation of the β-amino acid substrate so that the β-amino group of the substrate is placed adjacent to the Asp^{230} side-chain carboxyl group.

A comparison of the specificity-conferring code of VinN with other adenylation enzymes revealed that VinN has a special code for the β-amino acid substrate. The unique feature involves the presence of one polar residue, Ser^{299}, and two basic residues, Lys^{330} and Arg^{331} (corresponding to Ala^{301}, Ile^{330}, and Cys^{331}, respectively, in PheA). The crystal structure shows that all of these residues are involved in the recognition of the carboxyl group at the C1 position that is not adenylated (Fig. 2*B*). Other α-amino acid-activating enzymes generally have small aliphatic residues at the positions corresponding to Ser^{299} and Lys^{330} in VinN (3–7). In addition, they contain neither Arg nor Lys at the position equivalent to Arg^{331} in VinN, although they have various types of residues, including Asp and His, at this position. Thus, VinN has distinct amino acids at these positions. These polar and basic residues might be specific for the recognition of dicarboxylic β-amino acids. Even adenylation enzymes using dicarboxylic α-amino acid substrates, including L-aspartate and L-glutamate, have no basic residues at corresponding positions (7). These enzymes have a basic or polar residue at a different position such as the 234 or 278 position in PheA numbering for recognition of a carboxyl group that is not adenylated. Another feature is that VinN has a bulky aromatic residue, Phe^{231}, adjacent to the invariant Asp^{230}. The crystal structure shows that this Phe residue likely provides a steric constraint to control the substrate conformation. Normally, α-amino acid-activating enzymes have a small aliphatic residue such as Ala or Val at this position. Thus, the substrate-conferring code of VinN is quite different from those of α-amino acid adenylation enzymes. In contrast to VinN, SlgN1 shows the above mentioned α-amino acid adenylation enzyme-like features. SlgN1 contains Gln^{305} at the position equivalent to Thr^{278} in PheA (Fig. 5). The SlgN1 structure suggests that this polar Gln^{305} residue might be involved in carboxyl group recognition, although the structure of the complex with 3-MeAsp was not reported (26) (Fig. 4*D*). SlgN1 also has a small Ala^{264} residue adjacent to the invariant Asp^{263} residue. In addition, the length of the β13β14 loop in SlgN1 is the same as those in

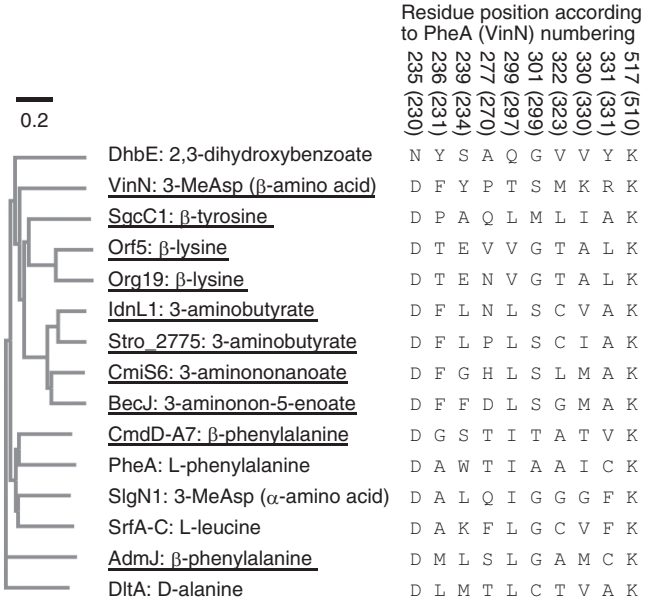

FIGURE 5. **Phylogenetic analysis of adenylation enzymes.** The sequences of the following 15 adenylation enzymes were used for the phylogenetic analysis: VinN, *B. subtilis* DhbE (41), *Streptomyces globisporus* SgcC1 (16), *Streptomyces rochei* Orf5 and Orf19 (24), *Streptomyces* sp. ML694-90F3 IdnL1 (18), *S. tropica* Stro_2775 (21), *Streptomyces* sp. MJ635-86F5 CmiS6 (19), *Streptomyces* sp. DSM 21069 BecJ (20), *Chondromyces crocatus* CmdD-A7 (17), *B. brevis* PheA (2), *S. lydicus* SlgN1 (26), *B. subtilis* SrfA-C (45), *Pantoea agglomerans* AdmJ (23), and *B. cereus* DltA (35). The specificity-conferring codes are also shown. VinN and other β-amino acid-activating enzymes are *underlined*.

α-amino acid-activating enzymes (Fig. 4*C*). These differences could explain why SlgN1 shows the opposite orientation of 3-MeAsp binding to VinN. A few alterations in the substrate-binding pocket affect the orientation of substrate in this case.

This study might be important from an evolutionary point of view. Adenylation enzymes might gain β-amino acid specificity from α-amino acid specificity with a few critical alterations of the substrate-binding pocket although they maintain the overall fold and catalytic mechanism. The replacement of some substrate-binding pocket residues is likely a key evolutionary event to generate various β-amino acid specificities. Sequence alignment and phylogenetic analysis show that other β-amino acid-activating enzymes can be divided into several subfamilies (Fig. 5). These enzymes possess an Asp residue at the position corresponding to Asp^{230} of VinN and are thought to use an Asp residue for the recognition of the β-amino group of the β-amino acid substrate in a manner similar to that of VinN. Of these, IdnL1 (18), CmiS6 (19), BecJ (20), and Stro_2775 (21), which use β-amino fatty acids in macrolactam antibiotic biosynthesis, might have a similar β-amino acid recognition mechanism because they share some residues in common with VinN. In particular, Phe^{231} and Ser^{299} of VinN are conserved in these enzymes (Fig. 5), which might use both the Phe and Ser residues to control substrate conformation by steric constraints similarly to VinN. In addition, these enzymes might have a β13β14 loop that is one residue shorter than that in α-amino acid-activating enzymes, although this is difficult to predict because of the low sequence identity (Fig. 4*C*). The identification of these conserved features could help the prediction of β-amino acid substrate specificity of biochemically uncharacterized adenylation enzymes on the basis of their amino acid sequences. Conversely, other types of β-amino acid-activating enzymes seem to use a different amino acid residue for recognition. For example, SgcC1, which activates β-tyrosine in C-1027 biosynthesis, contains a Pro residue adjacent to the invariant Asp (Fig. 5). This Pro residue is thought to be involved in the catalysis and/or specificity for β-amino acids as evidenced from mutational studies (16). Other enzymes have different amino acids in this position. CmdD-A_7, which activates β-phenylalanine in chondramide biosynthesis, has a smaller Gly residue (17), and Orf5, which activates β-lysine in streptothricin biosynthesis, contains a Thr residue (24). These enzymes might adopt a different strategy for β-amino acid recognition. The elucidation of the structures of these enzymes is necessary for the further understanding of β-amino acid recognition by adenylation enzymes.

In conclusion, we determined the first crystal structure of a β-amino acid adenylation enzyme. This structure sheds on the molecular basis for selective activation of β-amino acids by visualizing the orientation and conformation of the β-amino acid substrate. This study represents a significant contribution to the expansion of knowledge of the adenylation enzyme family. In addition, the VinN structure could provide clues useful for the protein engineering of an adenylation enzyme to enable alteration of the substrate specificity to introduce β-amino acids instead of α-amino acids.

Acknowledgments—We thank Dr. Takatoshi Arakawa at The University of Tokyo for assistance with the CD experiment. This work was performed with the approval of the Photon Factory Program Advisory Committee (Proposal 2012G0508).

REFERENCES

1. Gulick, A. M. (2009) Conformational dynamics in the acyl-CoA synthetases, adenylation domains of non-ribosomal peptide synthetases, and firefly luciferase. *ACS Chem. Biol.* **4,** 811–827
2. Conti, E., Stachelhaus, T., Marahiel, M. A., and Brick, P. (1997) Structural basis for the activation of phenylalanine in the non-ribosomal biosynthesis of gramicidin S. *EMBO J.* **16,** 4174–4183
3. Stachelhaus, T., Mootz, H. D., and Marahiel, M. A. (1999) The specificity-conferring code of adenylation domains in nonribosomal peptide synthetases. *Chem. Biol.* **6,** 493–505
4. Challis, G. L., Ravel, J., and Townsend, C. A. (2000) Predictive, structure-based model of amino acid recognition by nonribosomal peptide synthetase adenylation domains. *Chem. Biol.* **7,** 211–224
5. Rausch, C., Weber, T., Kohlbacher, O., Wohlleben, W., and Huson, D. H. (2005) Specificity prediction of adenylation domains in nonribosomal peptide synthetases (NRPS) using transductive support vector machines (TSVMs). *Nucleic Acids Res.* **33,** 5799–5808
6. Wackler, B., Lackner, G., Chooi, Y. H., and Hoffmeister, D. (2012) Characterization of the *Suillus grevillei* quinone synthetase GreA supports a nonribosomal code for aromatic α-keto acids. *ChemBioChem* **13,** 1798–1804
7. Khayatt, B. I., Overmars, L., Siezen, R. J., and Francke, C. (2013) Classification of the adenylation and acyl-transferase activity of NRPS and PKS systems using ensembles of substrate specific hidden Markov models. *PLoS One* **8,** e62136
8. Eppelmann, K., Stachelhaus, T., and Marahiel, M. A. (2002) Exploitation of the selectivity-conferring code of nonribosomal peptide synthetases for the rational design of novel peptide antibiotics. *Biochemistry* **41,** 9718–9726
9. Uguru, G. C., Milne, C., Borg, M., Flett, F., Smith, C. P., and Micklefield, J. (2004) Active-site modifications of adenylation domains lead to hydrolysis of upstream nonribosomal peptidyl thioester intermediates. *J. Am. Chem.*

Soc. **126,** 5032–5033
10. Stevens, B. W., Lilien, R. H., Georgiev, I., Donald, B. R., and Anderson, A. C. (2006) Redesigning the PheA domain of gramicidin synthetase leads to a new understanding of the enzyme's mechanism and selectivity. *Biochemistry* **45,** 15495–15504
11. Chen, C. Y., Georgiev, I., Anderson, A. C., and Donald, B. R. (2009) Computational structure-based redesign of enzyme activity. *Proc. Natl. Acad. Sci. U.S.A.* **106,** 3764–3769
12. Thirlway, J., Lewis, R., Nunns, L., Al Nakeeb, M., Styles, M., Struck, A. W., Smith, C. P., and Micklefield, J. (2012) Introduction of a non-natural amino acid into a nonribosomal peptide antibiotic by modification of adenylation domain specificity. *Angew. Chem. Int. Ed. Engl.* **51,** 7181–7184
13. Kudo, F., Miyanaga, A., and Eguchi, T. (2014) Biosynthesis of natural products containing β-amino acids. *Nat. Prod. Rep.* **31,** 1056–1073
14. Shinohara, Y., Kudo, F., and Eguchi, T. (2011) A natural protecting group strategy to carry an amino acid starter unit in the biosynthesis of macrolactam polyketide antibiotics. *J. Am. Chem. Soc.* **133,** 18134–18137
15. Mootz, H. D., and Marahiel, M. A. (1997) The tyrocidine biosynthesis operon of *Bacillus brevis*: complete nucleotide sequence and biochemical characterization of functional internal adenylation domains. *J. Bacteriol.* **179,** 6843–6850
16. Van Lanen, S. G., Lin, S., Dorrestein, P. C., Kelleher, N. L., and Shen, B. (2006) Substrate specificity of the adenylation enzyme SgcC1 involved in the biosynthesis of the enediyne antitumor antibiotic C-1027. *J. Biol. Chem.* **281,** 29633–29640
17. Rachid, S., Krug, D., Weissman, K. J., and Müller, R. (2007) Biosynthesis of (*R*)-β-tyrosine and its incorporation into the highly cytotoxic chondramides produced by *Chondromyces crocatus*. *J. Biol. Chem.* **282,** 21810–21817
18. Takaishi, M., Kudo, F., and Eguchi, T. (2013) Identification of incednine biosynthetic gene cluster: characterization of novel β-glutamate-β-decarboxylase IdnL3. *J. Antibiot.* **66,** 691–699
19. Amagai, K., Takaku, R., Kudo, F., and Eguchi, T. (2013) A unique amino transfer mechanism for constructing the β-amino fatty acid starter unit in the biosynthesis of the macrolactam antibiotic cremimycin. *ChemBioChem* **14,** 1998–2006
20. Jørgensen, H., Degnes, K. F., Sletta, H., Fjaervik, E., Dikiy, A., Herfindal, L., Bruheim, P., Klinkenberg, G., Bredholt, H., Nygård, G., Døskeland, S. O., Ellingsen, T. E., and Zotchev, S. B. (2009) Biosynthesis of macrolactam BE-14106 involves two distinct PKS systems and amino acid processing enzymes for generation of the aminoacyl starter unit. *Chem. Biol.* **16,** 1109–1121
21. Udwary, D. W., Zeigler, L., Asolkar, R. N., Singan, V., Lapidus, A., Fenical, W., Jensen, P. R., and Moore, B. S. (2007) Genome sequencing reveals complex secondary metabolome in the marine actinomycete *Salinispora tropica*. *Proc. Natl. Acad. Sci. U.S.A.* **104,** 10376–10381
22. Rouhiainen, L., Vakkilainen, T., Siemer, B. L., Buikema, W., Haselkorn, R., and Sivonen, K. (2004) Genes coding for hepatotoxic heptapeptides (microcystins) in the cyanobacterium *Anabaena* strain 90. *Appl. Environ. Microbiol.* **70,** 686–692
23. Fortin, P. D., Walsh, C. T., and Magarvey, N. A. (2007) A transglutaminase homologue as a condensation catalyst in antibiotic assembly lines. *Nature* **448,** 824–827
24. Maruyama, C., Toyoda, J., Kato, Y., Izumikawa, M., Takagi, M., Shin-ya, K., Katano, H., Utagawa, T., and Hamano, Y. (2012) A stand-alone adenylation domain forms amide bonds in streptothricin biosynthesis. *Nat. Chem. Biol.* **8,** 791–797
25. Shindo, K., Kamishohara, M., Odagawa, A., Matsuoka, M., and Kawai, H. (1993) Vicenistatin, a novel 20-membered macrocyclic lactam antitumor antibiotic. *J. Antibiot.* **46,** 1076–1081
26. Herbst, D. A., Boll, B., Zocher, G., Stehle, T., and Heide L. (2013) Structural basis of the interaction of MbtH-like proteins, putative regulators of nonribosomal peptide biosynthesis, with adenylating enzymes. *J. Biol. Chem.* **288,** 1991–2003
27. Webb, M. R. (1992) A continuous spectrophotometric assay for inorganic phosphate and for measuring phosphate release kinetics in biological systems. *Proc. Natl. Acad. Sci. U.S.A.* **89,** 4884–4887
28. Battye, T. G., Kontogiannis, L., Johnson, O., Powell, H. R., and Leslie, A. G. (2011) iMOSFLM: a new graphical interface for diffraction-image processing with MOSFLM. *Acta Crystallogr. D Biol. Crystallogr.* **67,** 271–281
29. Vagin, A., and Teplyakov, A. (2010) Molecular replacement with MOLREP. *Acta Crystallogr. D Biol. Crystallogr.* **66,** 22–25
30. Morris, R. J., Perrakis, A., and Lamzin, V. S. (2002) ARP/wARP and automatic interpretation of protein electron density maps. *Acta Crystallogr. D Biol. Crystallogr.* **58,** 968–975
31. Emsley, P., and Cowtan, K. (2004) Coot: model-building tools for molecular graphics. *Acta Crystallogr. D Biol. Crystallogr.* **60,** 2126–2132
32. Murshudov, G. N., Vagin, A. A., and Dodson, E. J. (1997) Refinement of macromolecular structures by the maximum-likelihood method. *Acta Crystallogr. D Biol. Crystallogr.* **53,** 240–255
33. DeLano, W. L. (2002) *The PyMOL Molecular Graphics System*, Schrödinger, LLC, New York
34. Lovell, S. C., Davis, I. W., Arendall, W. B., 3rd, de Bakker, P. I., Word, J. M., Prisant, M. G., Richardson, J. S., and Richardson, D. C. (2003) Structure validation by Cα geometry: φ, ψ and Cβ deviation. *Proteins* **50,** 437–450
35. Du, L., He, Y., and Luo, Y. (2008) Crystal structure and enantiomer selection by D-alanyl carrier protein ligase DltA from *Bacillus cereus*. *Biochemistry* **47,** 11473–11480
36. Villiers, B. R., and Hollfelder, F. (2009) Mapping the limits of substrate specificity of the adenylation domain of TycA. *ChemBioChem* **10,** 671–682
37. Reger, A. S., Wu, R., Dunaway-Mariano, D., and Gulick, A. M. (2008) Structural characterization of a 140° domain movement in the two-step reaction catalyzed by 4-chlorobenzoate:CoA ligase. *Biochemistry* **47,** 8016–8025
38. Goyal, A., Yousuf, M., Rajakumara, E., Arora, P., Gokhale, R. S., and Sankaranarayanan, R. (2006) Crystallization and preliminary x-ray crystallographic studies of the N-terminal domain of FadD28, a fatty-acyl AMP ligase from *Mycobacterium tuberculosis*. *Acta Crystallogr. Sect. F Struct. Biol. Cryst. Commun.* **62,** 350–352
39. Arora, P., Goyal, A., Natarajan, V. T., Rajakumara, E., Verma, P., Gupta, R., Yousuf, M., Trivedi, O. A., Mohanty, D., Tyagi, A., Sankaranarayanan, R., and Gokhale, R. S. (2009) Mechanistic and functional insights into fatty acid activation in *Mycobacterium tuberculosis*. *Nat. Chem. Biol.* **5,** 166–173
40. Goyal, A., Verma, P., Anandhakrishnan, M., Gokhale, R. S., and Sankaranarayanan, R. (2012) Molecular basis of the functional divergence of fatty acyl-AMP ligase biosynthetic enzymes of *Mycobacterium tuberculosis*. *J. Mol. Biol.* **416,** 221–238
41. May, J. J., Kessler, N., Marahiel, M. A., and Stubbs, M. T. (2002) Crystal structure of DhbE, an archetype for aryl acid activating domains of modular nonribosomal peptide synthetases. *Proc. Natl. Acad. Sci. U.S.A.* **99,** 12120–12125
42. Holm, L., and Sander, C. (1995) Dali: a network tool for protein structure comparison. *Trends Biochem. Sci.* **20,** 478–480
43. Yonus, H., Neumann, P., Zimmermann, S., May, J. J., Marahiel, M. A., and Stubbs, M. T. (2008) Crystal structure of DltA. Implications for the reaction mechanism of non-ribosomal peptide synthetase adenylation domains. *J. Biol. Chem.* **283,** 32484–32491
44. Nishio, M., Umezawa, Y., Fantini, J., Weiss, M. S., and Chakrabarti, P. (2014) CH-π hydrogen bonds in biological macromolecules. *Phys. Chem. Chem. Phys.* **16,** 12648–12683
45. Hughes, A. J., and Keatinge-Clay, A. (2011) Enzymatic extender unit generation for in vitro polyketide synthase reactions: structural and functional showcasing of *Streptomyces coelicolor* MatB. *Chem. Biol.* **18,** 165–176
46. Tanovic, A., Samel, S. A., Essen, L. O., and Marahiel, M. A. (2008) Crystal structure of the termination module of a nonribosomal peptide synthetase. *Science* **321,** 659–663
47. Lee, T. V., Johnson, L. J., Johnson, R. D., Koulman, A., Lane, G. A., Lott, J. S., and Arcus, V. L. (2010) Structure of a eukaryotic nonribosomal peptide synthetase adenylation domain that activates a large hydroxamate amino acid in siderophore biosynthesis. *J. Biol. Chem.* **285,** 2415–2427
48. Drake, E. J., Duckworth, B. P., Neres, J., Aldrich, C. C., and Gulick, A. M. (2010) Biochemical and structural characterization of bisubstrate inhibitors of BasE, the self-standing nonribosomal peptide synthetase adenylate-forming enzyme of acinetobactin synthesis. *Biochemistry* **49,** 9292–9305